Energy 61 (2013) 463–471

Contents lists available at ScienceDirect

Energy

journal homepage: www.elsevier.com/locate/energy

A 1D mathematical model for a microbial fuel cell

V.B. Oliveira [b, *], M. Simões [b], L.F. Melo [b], A.M.F.R. Pinto [a, *]

[a] CEFT, Departamento de Eng. Química, Universidade do Porto, Faculdade de Engenharia, Rua Dr. Roberto Frias, 4200-465 Porto, Portugal
[b] LEPAE, Departamento de Eng. Química, Universidade do Porto, Faculdade de Engenharia, Rua Dr. Roberto Frias, 4200-465 Porto, Portugal

ARTICLE INFO

Article history:
Received 8 March 2013
Received in revised form
30 June 2013
Accepted 28 August 2013
Available online 30 September 2013

Keywords:
Microbial fuel cells
Mathematical modelling
Heat and mass transfer
Biofilm
Bio-electrochemical
Simulation

ABSTRACT

MFCs (microbial fuel cells) are a promising sustainable technology to meet increasing energy needs, especially using wastewaters as substrates, since they can generate electricity and accomplish wastewater treatment simultaneously. The MFC is a complex system involving bio-electrochemical processes, charge, mass and energy transfer. In this work, a steady state, one-dimensional model accounting for coupled heat, charge and mass transfer, and biofilm formation, along with the electrochemical reactions occurring in the MFC, similar to the ones developed for chemical fuel cells, is presented. The model predicts the correct trends for the influence of current density on the cell voltage, as well as, the influence of substrate concentration and temperature on the MFC performance and biofilm thickness. The model outputs are the temperature and concentration profiles and the biofilm thickness. The proposed model is rapidly and easily implemented and is therefore suitable for inclusion in real-time system level MFC calculations.

1. Introduction

There is no effective way to keep us living on fossil fuels and reduce greenhouse emissions through increases in energy efficiency alone. Therefore, together with strong improvements in energy conservation and efficiency, new technologies are needed to gradually replace fossil sources by renewable ones [1–4].

Within the last years, the interest on MFCs (microbial fuel cells) has been growing, because they are able to simultaneously treat and produce electricity directly from the wastes that our society produces and can degrade toxic compounds and pollutants (phenol, sulfates and chromium). The MFCs operate at ambient temperatures, are fueled by organic matter which is neither toxic as methanol nor explosive as hydrogen and can contribute to optimize the overall efficiency of wastewater treatment facilities. This type of fuel cell share some similarities with chemical fuel cells, since in both cases the anode and cathode side are separated by a proton exchange membrane, the fuel is oxidized on the anode side and the oxidant (oxygen) reduced on the cathode side. However, MFC, use organic substrates as fuels to produce electricity and these organic compounds are catalysed by microorganism while in chemical fuel cells the fuel oxidation is catalysed by noble metals. As a result, electricity generation in a MFC is accomplished by microbial catabolism, electron transfer from microbes to the anode, reduction of electron acceptors at the cathode and proton transfer from the anode to the cathode.

Since, the microbial fuel cell is a multiphase system involving simultaneous biological and electrochemical processes, mass, charge and energy transfer, the development of a mathematical model is critical to the design and optimization of this type of cells. While novel materials are being developed to solve the above refereed problems, there is an urgent need for understanding and prediction of the main biological, mass and electrochemical processes. The development of mathematical models is a crucial tool for investigation system parameters and for the design and optimization of MFCs with reduced time and money. These models can be easily modified to simulate various configurations and operating conditions.

Modelling and simulation has been widely used to develop various chemical fuel cells systems and different types of approaches are available in literature [5,6]. Substantial information already exists on mass transfer, reactions and electrical phenomena, and this can be also adapted to MFCs. Despite the importance of MFCs modelling with the exception of one case over a decade ago [7], there have been, as far as we are aware, only a few modelling studies dedicated to MFCs [8–16] with different modelling approaches, areas of investigation and dimension of study. Table 1 categorizes the MFC models according to their areas of investigation and dimension of study.

* Corresponding authors.
E-mail addresses: vaniaso@fe.up.pt (V.B. Oliveira), apinto@fe.up.pt (A.M.F.R. Pinto).

0360-5442/$ – see front matter © 2013 Elsevier Ltd. All rights reserved.
http://dx.doi.org/10.1016/j.energy.2013.08.055

Table 1
MFC model categorization based on areas of investigation.

Feature	Reference									
	[7]	[8]	[9]	[10]	[11]	[12]	[13]	[14]	[15]	[16]
Dimension	1	1	3	3	2	1	1	1	1	1
Electrochemical	√	√	√	√	√	√	√	√	√	√
Dynamic	√	√	√	√	√		√	√	√	√
Mass transport	√	√	√	√	√		√	√	√	√
Biochemical	√	√	√	√	√		√	√	√	√
pH effects					√					
Biofilm		√	√	√	√				√	√
Multispecies		√	√	√	√				√	√
Cathode							√			
Anode	√	√	√	√	√			√	√	√

The more complex models are transport models using differential and algebraic equations whose derivation is based in the electrochemistry, biological and physics governing the phenomena taking place in the cell [8–11]. These equations are numerically solved by different computational methods, involving extensive calculations, but accurately predict all the phenomena occurring in the cell. The simpler ones are an adequate tool to understand the basic effect of different operating conditions and design parameters on MFC performance and can be used to predict voltage losses for simple designs and can be useful tool for rapid calculations [12–16]. However, they neglect some of crucial features such as transient performance and spatial non-uniformities. It should, also, be mentioned that most of the models developed for MFCs only considered the phenomena occurring in the anode side assuming an overpotential value for the cathode side. Therefore, all the important phenomena that occur on the cathode side which may affect the MFC performance are neglected [8–12,14–16] and can not be predicted by the model. As the authors are aware, only one work developed a coupled model for both anode and cathode chambers [13]. Based on the many similarities between the MFC and the other types of fuel cells (chemical fuel cells, like the direct methanol fuel cells) a one dimensional and analytical model of a two-chamber MFC was developed by Zeng et al. [13]. The model integrates the biochemical reactions, Butler–Volmer expressions and mass/charge balances and simulates both steady and dynamic behaviour of a MFC, including voltage, power density, fuel concentration, and the influence of various parameters on power generation. The proposed model is easy to implement and can serve as a framework for modelling other types of MFC and can contribute to the development and scale-up of more efficient MFCs. However, the major drawback of this work is that the biofilm formation on the anode side is not considered.

Due to the importance of the biofilm formation on the MFC anode electrode, recently computational models for biofilm based microbial fuel cells have been reported [8–11]. Although, these models provided detailed descriptions of multi-species for the biofilm anode by using partial differential equations, their practical application has inherent complexity, long computational times and may not be readily implemented by the majority of the MFC community.

To overcome that, simplified models consisting of ordinary differential equations that can adequately describe MFC microbial communities at various operating conditions while being suitable for process design and optimization are desirable.

Despite all the work done in MFC modelling [7–17], there is a lack of models describing the main biological, mass transfer, energy and charge effects in the anode and cathode compartment and taking into account the biofilm formation. Based on that and on the similarities above referred with chemical fuel cells and motivated by the successful development of two mathematical models for an active and passive DMFC (Direct methanol fuel cell) already published by Oliveira et al. [18,19], the objective of the present work is the development of a semi-analytical one-dimensional model considering the effects of coupled heat, charge, mass transfer and biofilm formation, along with the bio-electrochemical reactions occurring in MFCs. The model can be used to predict the effect of different operating and structural parameters on the MFC performance and biofilm formation. The aim of this work is to produce a simplified model describing the main processes occurring in a MFC fuel cell and reproducing with satisfactory accuracy experimental data.

2. Model development

A schematic representation of a microbial fuel cell is shown in Fig. 1, consisting of

- an anode chamber with an electron collector (electrode);
- a polymer electrolyte membrane (M);
- a cathode chamber with an electron collector (electrode);

In a MFC the fuel, wastewater, is supplied to the reaction zone by a liquid pump and the oxidant, air, by a mass flow controller. On the anode side a bio-electrochemical reaction occurs between microorganisms and a fuel/substrate which is oxidized releasing carbon dioxide, protons and electrons. The carbon dioxide (CO_2) produced moves counter-currently toward the anode exit, protons are transported to the cathode chamber through the membrane and electrons through an external electric wire. In the cathode, oxygen (O_2) reacts with protons and electrons generating water (H_2O). The water produced in the cathode moves counter-currently toward the cathode exit. The electrode reactions, considering acetate ($(CH_2O)_2$) as substrate, are:

Anode reaction:

$$(CH_2O)_2 + 2H_2O \rightarrow 2CO_2 + 8H^+ + 8e^- \quad (1)$$

Cathode reaction:

$$O_2 + 4H^+ + 4e^- \rightarrow 2H_2O \quad (2)$$

The model presented relies on the following assumptions:

- mass and heat transport are steady-state and one-dimensional (direction x in Fig. 1);
- the transport of heat and mass through the electrode layers and biofilm is assumed to be a diffusion dominated process and the convection effect is negligible;
- mass transport in the electrode and biofilm is described using effective Fick models;

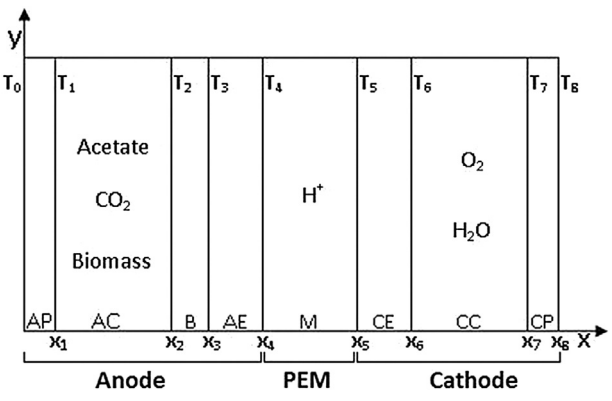

Fig. 1. Schematic representation of a MFC.

- the thermal energy model is based on the differential thermal energy conservation equation (Fourier's law);
- pressure gradient across the layers is negligible;
- only the liquid phase is considered in the anode side, so carbon dioxide remains dissolved in solution;
- local equilibrium at interfaces is represented by partition functions;
- the electrodes are assumed to be a macro-homogeneous porous electrode so reactions in these layers are modelled as a homogeneous reaction;
- anode kinetics is described by Tafel and Monod equations;
- the anodic and cathodic overpotential is constant through the catalyst layers;
- cathode kinetics is described by Tafel equation;
- the anode and cathode compartments are treated as a CSTR (continuous stirred tank reactor);
- mass balances, on the anode side, take into account rates of reactions in the anode compartment, biofilm and on the electrode;
- carbon dioxide, acetate and oxygen are assumed not to diffuse into the membrane;
- the steady-state biofilm is maintained through equilibrium between the overall rate of microbial growth through the substrate utilization and the overall rate of biomass losses [17];
- the heat generation by electrochemical reactions occurring in both electrodes, anode compartment and biofilm is considered;
- when compared with the heat generated by electrochemical reactions and overpotential, the heat released by joule effect is ignored;
- the anode and the cathode streams are acting as heat transfer fluids so they remove heat from the cell at their outlet temperatures;
- the temperatures of the external walls of the cell (T_0 and T_8 in Fig. 1) are known;
- the heat flux generated in the electrodes, anode compartment and biofilm is assumed to be constant.

2.1. Mass transport

The anode compartment is treated as a CSTR (continuous stirred tank reactor), so the mass balance for acetate and biomass is described by

$$N_A = \frac{q^{AF}}{A^S}\left(C_A^0 - C_A^{AC}\right) \tag{3}$$

$$N_A = \frac{V^{AC}K_{\mathrm{dec}}C_X}{A^S Y_{X/A}} - \frac{q^{AF}}{A^S f_X Y_{X/A}}\left(C_X^0 - C_X\right) \tag{4}$$

where K_{dec} is decay rate, $Y_{X/A}$ is the bacterial yield and f_x is the reciprocal of wash-out fraction.

In the biofilm layer the mass balance is related to the concentration gradient assuming Fickian diffusion [20] with an effective diffusivity$D_A^{\mathrm{eff},B}$. The acetate flux can be determined from:

$$N_A = -D_A^{\mathrm{eff},B}\frac{dC_A^B}{dx} \tag{5}$$

It is assumed that the steady-state biofilm is maintained through equilibrium between the overall rate of microbial growth through the substrate utilization and the overall rate of biomass losses from the decay. The microbial growth rate based on the substrate utilization is expressed as the flux of substrate at the external surface of the biofilm ($N_A|_{x=x_2}$ or $N_A|_{x=x_3}$). For an idealized biofilm, the microbial composition (C_x) is uniform over the entire biofilm thickness so the biomass loss rate is expressed as $K_{\mathrm{dec}}C_x\delta_B$ [17]. At steady sate, setting the two rates equal gives:

$$K_{\mathrm{dec}}C_X\delta_B = N_A|_{x=x_2} \text{ or } K_{\mathrm{dec}}C_X\delta_B = N_A|_{x=x_3} \tag{6}$$

where:

$$N_A|_{x=x_2} = \frac{q^{AF}}{A^S}\left(C_A^0 - C_A^{AC}\right) \tag{7}$$

and

$$N_A|_{x=x_3} = -D_A^{\mathrm{eff},AE}\frac{dC_A^{AE}}{dx} \tag{8}$$

In the anode electrode, the mass balance is related to the concentration gradient assuming Fickian diffusion [20] with an effective diffusivity $D_A^{\mathrm{eff},AE}$.

The concentration at the *AC*/*B*, *B*/*AE* and *AE*/*M* interfaces is given by assuming local equilibrium with partition coefficients, K_2, K_3 and K_4. The boundary conditions for Eqs. (5) and (8) are (see Fig. 1)

$$\text{At } x = x_2: \quad C_{2,A}^B = K_2 C_A^{AC} \tag{9}$$

$$\text{At } x = x_3: \quad C_{3,A}^{AE} = K_3 C_{3,A}^B \tag{10}$$

$$\text{At } x = x_4: \quad C_A^M = K_4 C_{4,A}^{AE} = 0 \tag{11}$$

It is assumed that no acetate passes through the membrane to the cathode side, so the acetate concentration in *AE*/*M* interface is zero.

In fuel cells, all the fluxes can be related to a single characteristic flux, the current density or charge flux of the fuel cell. In the MFC, the acetate flux is related to the current density by:

$$N_A = \frac{3600 I_{\mathrm{Cell}}}{8F} \tag{12}$$

where 3600 is the unit conversion factor.

At the anode side, acetate degradation/oxidation is a bio-electrochemical reaction, so to formulate the reaction rate equation both effects (biological degradation and electrochemical reaction) should be included. To describe the biological degradation a Monod-type approach was used and the electrochemical effect is modelled using Tafel equation. It should also, be mentioned that on the anode side the electrons are produced in both reactions occurring on the anode compartment and biofilm. The anode reaction rate is given by:

$$N_A = k\exp\left(\frac{\alpha_a\eta_a F}{RT}\right)\frac{C_A^{AC}}{K_A + C_A^{AC}}C_X + k\exp\left(\frac{\alpha_a\eta_a F}{RT}\right)\frac{C_A^{AB}}{K_A + C_A^{AB}}C_X \tag{13}$$

where k is the rate constant, K_A is the half velocity rate constant for acetate, the first term describes the electrons production on the anode compartment and the second the electrons production on the biofilm.

Like at the anode side, the cathode compartment is treated as a CSTR (continuous stirred tank reactor), so the oxygen flux is described by:

$$N_{O_2} = \frac{q^{CF}}{A^S}\left(C_{O_2}^0 - C_{O_2}^{CC}\right) \tag{14}$$

In the cathode electrode, oxygen flux is related to the concentration gradient by assuming Fickian diffusion [20] with an effective diffusivity $D_{O_2}^{eff,CE}$. The flux can be determined from:

$$N_{O_2} = -D_{O_2}^{eff,CE}\frac{dC_{O_2}^{CE}}{dx} \quad (15)$$

It is assumed that there is no oxygen crosses the membrane to the anode side, so the oxygen concentration in CE/M interface is zero. The concentration at the M/CE and CE/CC interfaces is given by assuming local equilibrium with a partition coefficient K_5 and K_6. The boundary conditions for Eq. (15) are:

$$\text{At } x = x_5: \quad C_{O_2}^{M} = K_5 C_{5,O_2}^{CE} = 0 \quad (16)$$

$$\text{At } x = x_6: \quad C_{6,O_2}^{CE} = K_6 C_{O_2}^{CC} \quad (17)$$

At the cathode catalyst layer, the oxygen reacts with the electrons and protons to produce water. Therefore the oxygen flux is related to the current density by:

$$N_{O_2} = \frac{3600 I_{Cell}}{4F} \quad (18)$$

At the cathode, the electrochemical reaction is modelled using Tafel equation for the oxygen reduction. The cathode overpotential can then be determined from:

$$I_{Cell} = I_{0,ref}^{O_2}\frac{C_{O_2}^{CE}}{C_{O_2,ref}^{CE}}\exp\left(\frac{\alpha_c \eta_c F}{RT}\right) \quad (19)$$

where $I_{0,ref}^{O_2}$ is the exchange current density of oxygen and $C_{O_2,ref}^{CE}$ is the reference concentration of oxygen.

2.2. Heat transport

Based on the simplifications and assumptions described previously the following overall heat transfer equation can be proposed (see Fig. 1):

$$Q_{generated}^{AC} + Q_{generated}^{B} + Q_{generated}^{AE} + Q_{generated}^{CE} = Q_1 + Q_4 + Q^{AF} + Q^{CF} \quad (20)$$

where Q^{AF} and Q^{CF} represent the heat transferred to the anode and cathode stream. The total heat generated in the MFC (anode compartment, biofilm and anode and cathode electrode) is equal to the heat losses to the surrounding environment at the anode and cathode side (Q_1 and Q_4 respectively) plus the heat removed by the anode and cathode fuel streams.

Complementarily, the following heat transfer balances can be written:

$$Q^{AF} = Q_{generated}^{AC} \quad (21)$$

$$Q_3 = Q_2 + Q_{generated}^{CE} \quad (22)$$

$$Q_3 = Q^{CF} \quad (23)$$

$$Q_4 = Q_3 - Q^{CF} \quad (24)$$

The energy balance for the anode and cathode streams, considering a steady-flow system with one inlet and one outlet, where the changes in kinetic and potential energies are negligible and there is no work interaction, are, respectively,

$$Q^{AF} = \frac{q^{AF}\rho^{AF}Cp^{AF}}{A^S}(T_2 - T_{AF}) \quad (25)$$

$$Q^{CF} = \frac{q^{CF}\rho^{CF}Cp^{CF}}{A^S}(T_7 - T_{CF}) \quad (26)$$

where ρ^{AF} and ρ^{CF} are the specific weights of the anode and cathode streams and Cp^{AF} and Cp^{CF} the specific heat capacity for anode and cathode streams, respectively.

At the anode, heat generated by the electrochemical reaction is given by

$$Q_{generated}^{i} = I_{Cell}\eta_a - I_{Cell}\left(\frac{\Delta H_a^i - \Delta G_a^i}{8F}\right) \quad (27)$$

where i represents AC, B or AE.

In this equation the first term represents the heat due to the activation and mass transfer overpotentials at the anode and the second term represents the entropy change of the anodic electrochemical reaction, with ΔH_a (difference between the enthalpies of products and reactants on the anodic reaction) denoting the anodic reaction enthalpy and ΔG_a (difference between the Gibbs free energy of products and reactants on the anodic reaction) the Gibbs free energy, which depend on the temperature of each layer.

In a similar way, the heat generated at the CE, can be determined from

$$Q_{generated}^{CE} = I_{Cell}\eta_c - I_{Cell}\left(\frac{\Delta H_c - \Delta G_c}{4F}\right) \quad (28)$$

where the first term represents the heat due to the activation and mass transfer overpotentials and the second term represents the entropy change of the cathodic electrochemical reaction, with ΔH_c (difference between the enthalpies of products and reactants on the cathodic reaction) denoting the cathodic reaction enthalpy and ΔG_c, the Gibbs free energy (difference between the Gibbs free energy of products and reactants on the cathodic reaction).

In the anode and cathode end plate and membrane the heat flux Q_1, Q_2 and Q_4 can be related to the temperature gradient across each layer, using the Fourier's law, as

$$Q = -K^l\frac{dT}{dx} \quad (29)$$

where l represents AP, CP, or M

On the cathode compartment the heat flux Q_3 can be related to the temperature gradient across this layer, using Newton's law, as

$$Q_3 = -h^{CC}A^S\Delta T \quad (30)$$

where h^{CC} is the heat transfer coefficient due to forced convection and can be determined from Ref. [21]:

$$Nu = \frac{h^{CC}L}{K^{CF}} = 0.664\mathrm{Re}^{1/2}\mathrm{Pr}^{1/3} \quad (31)$$

where Re is the Reynolds number ($\mathrm{Re} = (\nu^{CF}\rho^{CF}Cp^{CF})/\mu^{CF}$) and Pr the Prandtl number ($\mathrm{Pr} = (\mu^{CF}Cp^{CF})/K^{CF}$).

The differential equations describing the temperature profiles in the anode and cathode electrode and Biofilm are:

$$\frac{d^2T}{dx^2} = \frac{Q^B}{K^B\delta^B} \quad (32)$$

$$\frac{d^2T}{dx^2} = \frac{Q^{AE}}{K^{AE}\delta^{AE}} \tag{33}$$

$$\frac{d^2T}{dx^2} = \frac{Q^{CE}}{K^{CE}\delta^{CE}} \tag{34}$$

where Q^B, Q^{AE} and Q^{CE} are, respectively, the heat generated in the biofilm, anode electrode and cathode electrode.

The boundary conditions for Eqs. (32)–(34) are the temperatures at the walls (T_2, T_3, T_4, T_5 and T_6).

For the anode and cathode electrode, Fourier's law gives

$$\text{At } x = x_4: \quad Q_2 = K^{AE}\frac{dT}{dx} \tag{35}$$

$$\text{At } x = x_5: \quad Q_4 = -K^{CE}\frac{dT}{dx} \tag{36}$$

where dT/dx is calculated using the temperature profile obtained from the integration of equations (33) and (34).

2.3. Cell performance

The determination of acetate, biomass and oxygen concentrations at the electrodes, the temperature profiles and the anodic and cathodic overpotentials from the model equations enables prediction of the cell voltage, which can be expressed as:

$$V_{\text{Cell}} = E_{\text{Cell}} - \eta_a - \eta_c - I_{\text{Cell}}R_{\text{Cell}} \tag{37}$$

η_a and η_c are the anode and cathode overpotentials and account for both the activation loss and the concentration loss on the anode and cathode side. The fourth term on the right hand side represents the ohmic loss [18,19,22]. The membrane resistance R_{Cell} is given by

$$R_{\text{Cell}} = \frac{\delta^M}{\kappa} \tag{38}$$

where δ^M is membrane thickness and κ is the ionic conductivity of the membrane.

The results presented in the next section were obtained based on the parameters listed in Table 2. All parameters were carefully chosen from recent literature, namely the reference exchange current density and the transfer coefficients. In numerous published works, there are numerous values for the same parameter and it seems that some authors use the parameters that better fit their experimental results and not the most adequate to their operating/design conditions. All parameters presented in Table 2 were chosen based on recommendations from two recent specific works for anode and cathode kinetics [13,18,19].

3. Results and discussion

The developed model coupling biological, heat and mass transfer processes occurring in the MFC is rapidly implemented with simple numerical tools: Matlab and Excel.

In this section, examples of model predictions obtained after implementation of the model are presented. The conditions chosen to generate the simulations are similar to those used by Zeng et al. [13] in their experiments. This work was selected since the authors give complete reporting data essential to use in the present model.

Table 2
Parameter values.

q^{AF}	2.25×10^{-5} m^3/h	[13]
V^{AC}, V^{CC}	5.5×10^{-5} m^3	[13]
C_A^0	1.56 mol/m^3	[13]
k	0.207 mol/(m^{3}h)	[13]
α_a	0.051	[13]
T_0, T_8	303 K	assumed
T^{AF}, T^{CF}	303 K	assumed
K_A	0.592 mol/m^3	[13]
f_x	10	[13]
C_X^0	0 mol/m^3	[13]
$Y_{X/A}$	0.05	[8]
K_{dec}	8.33×10^{-4} h^{-1}	[13]
A^S	5×10^{-4} m^2	[13]
$D_A^{\text{eff},AE}$	$\varepsilon^{AE^{2.5}}(1.1 \times 10^{-9} \times 3600)$ m^2/h	[11]
$D_A^{\text{eff},B}$	$0.8 \times (1.1 \times 10^{-9} \times 3600)$ m^2/h	[8]
ε^{AE}, ε^{CE}	0.86	[18]
δ^{AE}, δ^C	0.000023 m	assumed
K_{2-6}	0.8	assumed
δ^{AC}, L	0.1 m	assumed
$D_{O_2}^{\text{eff},CE}$	$\varepsilon^{CE^{2.5}}[(T^{1.75} \times 5.8 \times 10^{-4})/(27.772 \times P)] \times 3600 \times 10^{-4}$ m^2/h	[18]
$C_{O_2}^0$	$(0.21 \times P)/(R \times T)$ mol/m^3	assumed
$C_{O_2,\text{ref}}^{CE}$	$(0.21 \times P)/(R \times T)$ mol/m^3	[18]
$I_{0,\text{ref}}^{O_2}$	$4.222 \times 10^{-2} exp((73200/R)(1/353 - 1/T))$ A/m^2	[18]
P	1 atm	assumed
q^{CF}	1.11×10^{-3} m^3/h	[13]
α_c	0.44	assumed
K^{AP}, K^{CP}	0.2 W/mK	[21]
K^M	0.43 W/mK	[13]
K^B	$0.8 \times K_{\text{water}}$ W/mK	assumed
K^{AE}	$(1 - \varepsilon^{AE}) \times 98 + \varepsilon^{AC}K_{\text{water}}$ W/mK	assumed
K^{CE}	$(1 - \varepsilon^{CE}) \times 0.15 + 0.07 \times 71 + \varepsilon^{CE}K_{\text{air}}$ W/mK	[18]
E_{Cell}	0.77 V	[13]
κ	3.6 S/m^2	[18]
δ^M	1.778×10^{-4} m	[18]

3.1. Model validation and sensitivity analysis

In Fig. 2, the predictions from the developed model and from the model described by Zeng et al. [13] are presented. Comparing the two approaches it can be seen that both predictions are generally in good accordance with the experimental data. The present model, however, predicts better the performance of the MFC cell studied by Zeng et al. [13] mainly at low to moderate

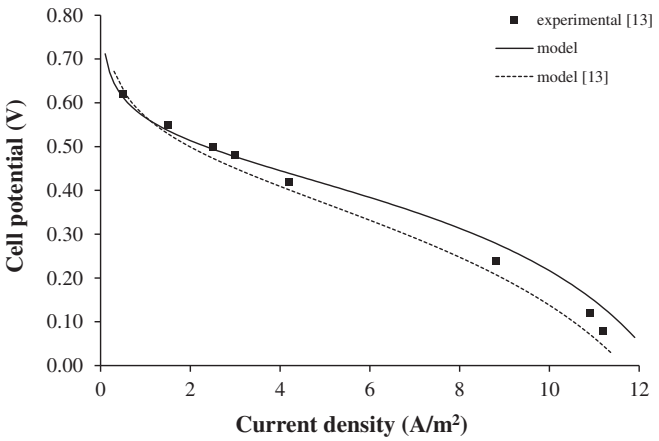

Fig. 2. Comparison of the presented model predictions and those proposed by Zeng et al. [13]; dots: experimental data from Ref. [13], lines: model predictions. Operating conditions: acetate concentration 1.56 mol/m^3, temperature 30 °C.

Table 3
Percentage changes in cell voltage when each assumed parameter is varied.

Ratio	Parameter				
	α_a	K_A	k	α_c	K_6
0.8	−4.09	−15.73	33.16	33.03	3.84
1.2	6.14	18.36	−34.19	−39.12	−4.70

current densities, probably due to the introduction of the heat transfer effects and mass transfer effects on biofilm and on the anode and cathode electrode. The open-circuit voltage, predicted by the model, is lower than the thermodynamic equilibrium cell voltage and this prediction is in accordance with experimental observations [13]. This decrease in cell voltage is due to three irreversible losses that occur in fuel cells: the activation overpotential, the ohmic loss and the concentration polarization. The activation polarization is dominant at low current densities and is due to an activation energy that must be overcome by the reacting species. Phenomena involving adsorption or desorption of reactant species, transfer of electrons and the nature of the electrode surface contribute to the activation polarization. In the middle of the operating range, the predominant loss is the Ohmic loss which is due to ionic and electronic conduction. At very high current densities, the major loss is the concentration polarization which is due to the inability to maintain the initial substrate concentration in the bulk fluid and to mass transport limitations. Polarization curves of a MFC illustrate the various losses and the extent of each one, pointing out possible measures to minimize them. These measures include selection of new microbes, mediators and substrates, modifications in the MFC design and using different operating conditions.

In the present work, as explained in the previous section, all parameters were carefully chosen according to the operating conditions and following the suggestions of literature [13,18,19]. However a basic parametric analysis on the model parameters was performed and the results can be found in Table 3. The major goal of this analysis is to evaluate which parameters are critical for a good prediction. Based on that, each model parameter (α_a, K_A, k, α_c, K_2, K_3, K_4, K_5, K_6) was varied one at a time by multiplying the ratio (0.8 and 1.2) to its original value (see Table 2), while leaving the other parameters unchanged. The resultant average percentage changes in the cell voltage over the range of current density (1–12 A/m^2) are presented in Table 3 with the exception of parameters K_2, K_3, K_4, K_5 since its values are approximately zero. As shown in Table 3 , when each parameter is reduced by a factor of 0.8, the rate constant of the anode reaction and the cathodic transfer coefficient lead to the largest increase in the cell voltage over the entire range of cell current density, there are an absolute change of 33% for the last one. When the parameter is increased by a factor of 1.2 these two parameters show, also, the largest changes, a decrease of, respectively, 34% and 39%. These results show that these two parameters are critical to the accuracy of the model predictions. The third largest change both for an increase of 1.2 and a decrease of 0.8 on its value is the half rate constant for acetate with, respectively a decrease on the cell voltage of 16% and an increase of 18%. Based on their results the impacts of both anodic transfer coefficient and the partition coefficient K_6 are not significant to the model accuracy.

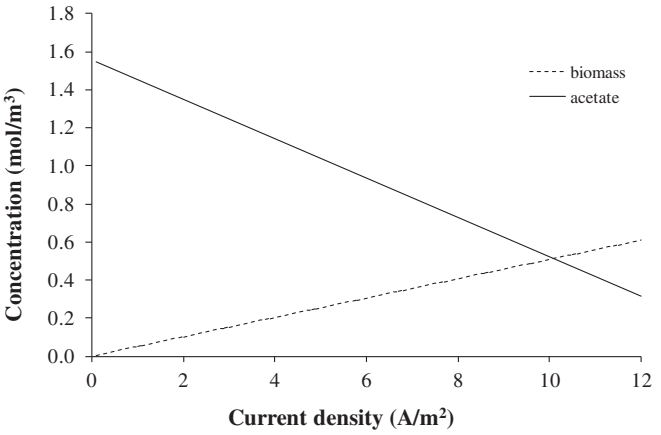

Fig. 4. Model predictions of biomass and acetate concentration for different current densities. Operating conditions: acetate concentration 1.56 mol/m^3, temperature 30 °C.

3.2. Model simulations

Fig. 3 shows the prediction of the anode and cathode overpotential as a function of current density. As can be seen, both curves increase with an increase of current density and the cathode overpotential curve is always higher that the anode curve. This shows that the cathodic reaction is the most significant factor limiting the performance of a MFC. These results are in accordance to those proposed by Zeng et al. [13]. It can be also observed that the increase of the cathode overpotential is higher for low current

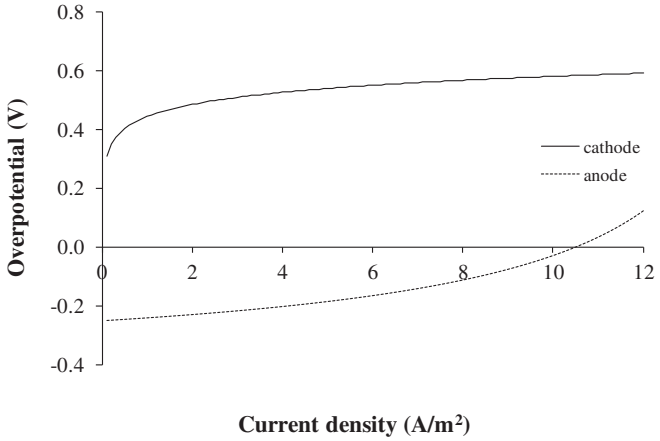

Fig. 3. Model predictions for anode and cathode overpotentials for different current densities. Operating conditions: acetate concentration 1.56 mol/m^3, temperature 30 °C.

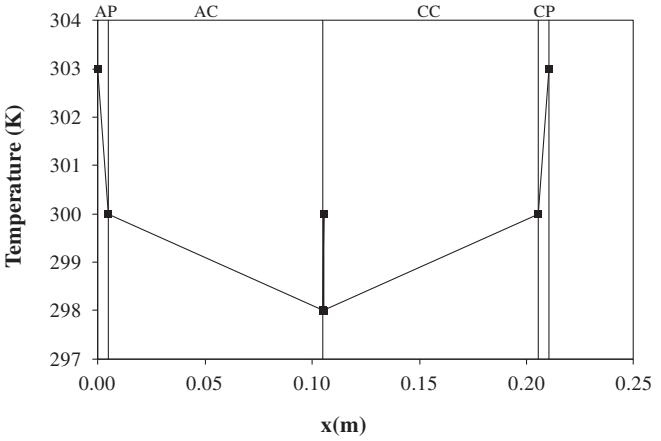

Fig. 5. Prediction for the temperature distribution in the cell for a current density of 5 A/m^2. Operating conditions: acetate concentration 1.56 mol/m^3, temperature 30 °C.

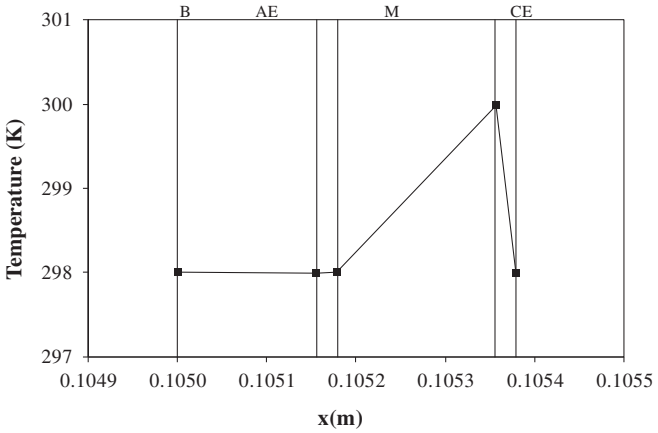

Fig. 6. Prediction for the temperature distribution in biofilm, anode electrode, cathode electrode and membrane for a current density of 5 A/m^2. Operating conditions: acetate concentration 1.56 mol/m^3, temperature 30 °C.

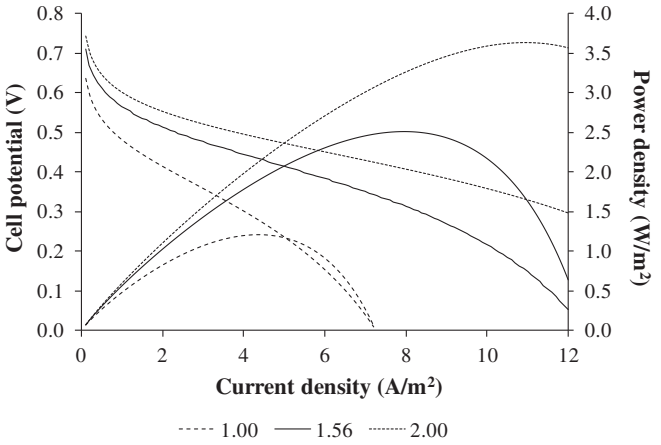

Fig. 8. Influence of acetate concentration on the cell voltage and power density. Operating conditions: temperature 30 °C.

densities, where the major loss presented is the activation overpotential. This indicate that the lost of performance in this region is mainly due to the cathode reaction. To improve the cathodic reaction the development of more efficient cathode materials is fundamental. For high current densities, where the major loss is the concentration polarization, the increase of the anode overpotential is higher than the cathode. These results show that the contribution of the anode overpotential for the cell voltage loss is higher, in this region. This is due to a decrease of the substrate concentration on the reaction media as can be seen in Fig. 4.

The predicted concentration of biomass and acetate in the anode compartment are presented in Fig. 4. As can be seen, and as expected, the acetate concentration decreases and the biomass concentration increases for an increase on the current density. Indeed, a higher current density leads to an increase on the reaction rate which consumes more acetate.

Figs. 5 and 6 show, respectively, the temperature distribution in the cell and in the active section of the cell (biofilm, anode electrode, membrane and cathode electrode) for a current density of 5 A/m^2. The data points represent the temperatures at the several layer interfaces. It is seen from Fig. 6 that, under the presented operating conditions, the temperature in the anode side is slightly lower than that in the cathode. This is due to the fact that the cathode reaction is exothermal, realising heat to the system and consequently increasing temperature.

Fig. 7 shows the predictions of the biofilm thickness as a function of current density. As can be seen in this Figure, the biofilm thickness decreases with an increase of the current density. As referred in the model assumptions the steady-state biofilm is maintained through equilibrium between the overall rate of microbial growth through the substrate utilization and the overall rate of biomass losses [17]. An increase on the current density leads to an increase on the anode reaction rate and consequently a decrease of the substrate concentration. Since the utilization of substrate decreases and based on the model assumption, the biofilm thickness, also, decreases.

Model predictions for the effect of substrate concentration on MFC voltage and power output can be found in Fig. 8. The plots from this figure show that higher substrate concentration yields a higher power output and cell voltage. As already mentioned, electron transfer to the anode by electrochemically active microorganisms is a result of primary metabolism, so the relationship between substrate concentration and current generation follows Monod's equation under conditions where the microorganisms can function without any limitations. Increases in substrate concentration therefore lead to increased current production and power output.

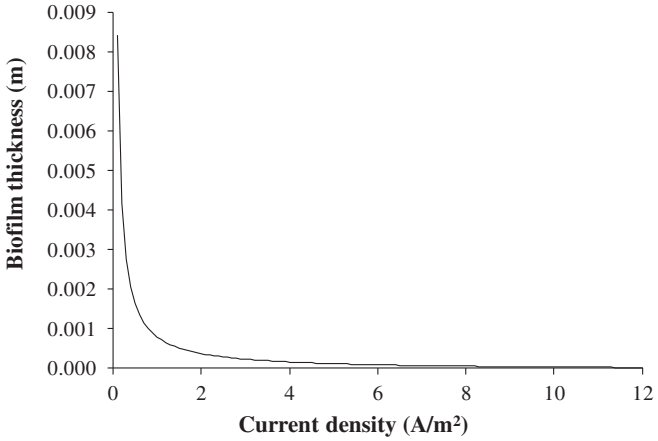

Fig. 7. Model predictions for the biofilm thickness for different current densities. Operating conditions: acetate concentration 1.56 mol/m^3, temperature 30 °C.

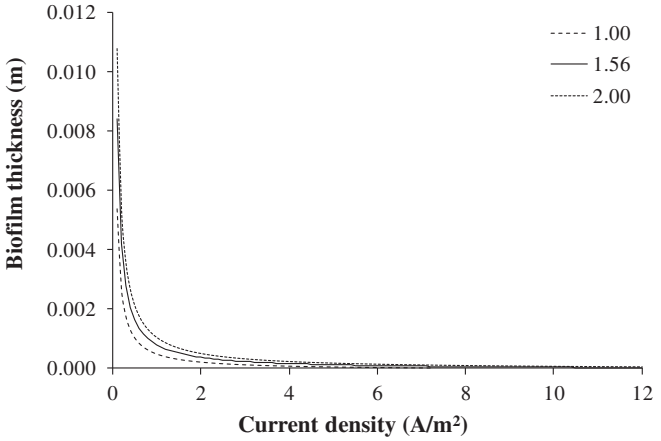

Fig. 9. Influence of acetate concentration on biofilm thickness for different current densities. Operating conditions: temperature 30 °C.

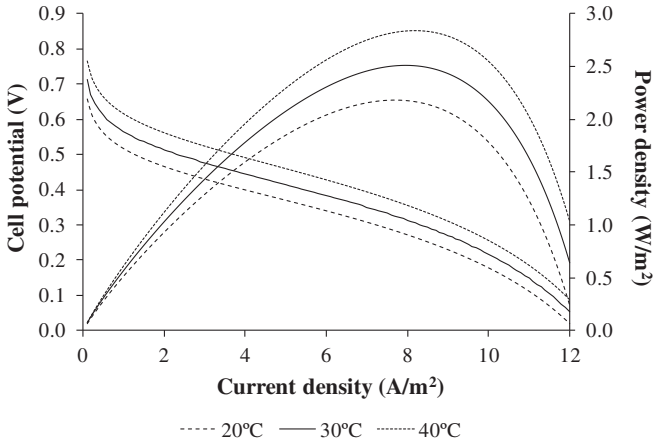

Fig. 10. Model predictions for the effect of temperature on the cell voltage and power density. Operating conditions: acetate concentration 1.56 mol/m^3.

The model predictions for the effect of the substrate concentration on the biofilm thickness are presented in Fig. 9. As can be seen, the substrate concentration has a slightly effect on the biofilm thickness, since an increase on the concentration leads to an increase of the biofilm thickness. As already mentioned, the biofilm is maintained through equilibrium between the overall rate of microbial growth through the substrate utilization and the overall rate of biomass losses. Higher substrate concentrations lead to an increase on the microbial growth rate through the substrate utilization so the biofilm thickness also, increases.

Model simulations for the effect of temperature on MFC performance are presented in Fig. 10. As can be seen, an increase on temperature leads to an increase of the cell voltage and power density. This fact may be due to the enhancement of membrane permeability, to the Ohmic resistance reduction due to higher conductivity of the liquid solution and to an increase of the microbial metabolism with temperature.

4. Conclusions

A simple, using low CPU (central processing unit), steady-state, one-dimensional model accounting for coupled heat, charge and mass transfer occurring in a MFC fuel cell is presented. The model outputs are the temperature and concentration across the cell and the biofilm thickness. The model allows the assessment of the effect of operating parameters (such as fuel and oxygen feed concentration, flow-rate and temperature) and the design parameters (active area and material properties) on the biofilm thickness and on the temperature and concentration profiles along the cell and consequently on the cell performance.

The set of parameters used in the present model predictions was rationally chosen according to operating conditions and following recommendations from literature. Model predictions were successfully compared to experimental and theoretical *I*–*V* polarization curves presented by Zeng et al. [13]. The model predicts the correct trends of the influence of current density on the anode and cathode overpotential, on the biofilm thickness, temperature and concentration profiles. With this easy to implement model, suitable operating conditions and design parameters can be set-up in order to achieve the power outputs needed for real applications.

The presented model is a useful tool to improve MFC understanding and to optimize fuel cell design and operation. This easily to implement reduced model is suitable for use in real-time MFC simulations.

Acknowledgements

V.B. Oliveira acknowledges the post-doctoral fellowship (SFRH/BDP/66837/2009 and SFRH/BDP/91993/2012) supported by the Portuguese “Fundação para a Ciência e Tecnologia” (FCT), POPH/QREN and European Social Fund (ESF). POCI (FEDER) also supported this work via CEFT and LEPAE.

Nomenclature

AC	anode compartment
AE	anode electrode
AP	anode acrylic plate
A^S	surface area of the membrane, m^2
B	biofilm
C	concentration, mol/m^3
C_2	concentration at the AC/B interface, mol/m^3
C_3	concentration at the B/AE interface, mol/m^3
C_4	concentration at the AE/membrane interface, mol/m^3
C_5	concentration at the membrane/CE interface, mol/m^3
C_6	concentration at the CE/CC interface, mol/m^3
CC	cathode compartment
CE	cathode electrode
CP	cathode acrylic plate
$C_{O_2,ref}$	reference concentration of oxygen, mol/m^3
Cp	specific heat capacity, J/(molK)
D^{eff}	effective diffusion coefficient, m^2/h
E_{Cell}	thermodynamic equilibrium potential, *V*
F	Faraday’s constant, 96,500 C/mol
f_x	reciprocal of wash-out fraction
G	Gibbs free energy, J/mol
H	enthalpy of reaction, J/mol
I_{Cell}	cell current density, A/m^2
$I_{0,ref}^{O_2}$	exchange current density of oxygen, A/m^2
k	constant in the rate expression (Eq. (13)), mol/(m^{3}h)
K_{2-6}	partition coefficients
K	thermal conductivity, W/(mK)
K_A	half velocity rate constant for acetate, mol/m^3
K_{dec}	decay rate, h^{-1}
M	membrane
N	molar flux, mol/(m^{2}h)
P	pressure of air in cathode, atm
PEM	polymer electrolyte membrane
q	flow rate, m^3/h
Q^{AF}	heat transfer to the anode stream, W/m^2
Q^{CF}	heat transfer to the cathode stream, W/m^2
Q	heat transfer, W/m^2
R	gas constant, 8.314 J/(molK)
R_{Cell}	internal resistance of the fuel cell, m^2/S
T	temperature, K
T_0	wall temperature at the anode side, K
T_8	wall temperature at the cathode side, K
$Y_{X/A}$	bacterial yield
V	volume, m^3
V_{Cell}	cell voltage, *V*
x	coordinate direction normal to the anode, *m*

Greek

Δ	variation
α_a	anodic transfer coefficient
α_c	cathodic transfer coefficient
δ	thickness, m
ε	porosity

η_a	anode overpotential, V
η_c	cathode overpotential, V
κ	ionic conductivity of the membrane, S/m
μ	dynamic viscosity, kg/(ms)
ν	velocity, m/s ($\nu = q/A$)
ρ	density, kg/m^3

Subscripts

A	acetate
air	air
water	water
O_2	oxygen
X	biomass

Superscripts

0	feed conditions
AC	anode compartment
AE	anode electrode
AF	anode flow
AP	anode acrylic plate
B	biofilm
CC	cathode compartment
CE	cathode electrode
CF	cathode flow
CP	cathode acrylic plate
i	layer i
l	layer l
M	membrane

References

[1] Powel EE, Hill GA. Carbon dioxide neutral, integrated biofuel facility. Energy 2010;35:4582–6.
[2] Song G, Xiao J, Zhao H, Shen L. A unified correlation for estimating specific chemical exergy of solid and liquid fuels. Energy 2012;40:164–73.
[3] Chatzifragkou A, Makri A, Belka A, Bellou S, Mavrou M, Mastoridou M, et al. Biotechnological conversions of biodiesel derived waste glycerol by yeast and fungal species. Energy 2011;36:1097–108.
[4] Posada JA, Cardona CA. Design and analysis of fuel ethanol production from raw glycerol. Energy 2010;35:5286–93.
[5] Oliveira VB, Falcão DS, Rangel CM, Pinto AMFR. A comparative study of approaches to direct methanol fuel cells modeling. Int J Hydrogen Energy 2007;32:415–24.
[6] Bavarian M, Soroush M, Kevrekidis IG, Benziger JB. Mathematical modeling, steady-state and dynamic behavior, and control of fuel cells: a review. Indus Eng Chem Res 2010;49:7922–50.
[7] Zhang XC, Halme A. Modelling of a microbial fuel cell process. Biotechnol Lett 1995;17:809–14.
[8] Marcus AK, Torres CI, Rittman BE. Conduction-based modeling of the biofilm anode of a microbial fuel cell. Biotechnol Bioeng 2007;98:1171–82.
[9] Picioreanu C, Head IM, Katuri KP, Van Loosdrecht MCM, Scott K. A computational model for biofilm-based microbial fuel cells. Water Res 2007;41:2921–40.
[10] Picioreanu C, Head IM, Katuri KP, Van Loosdrecht MCM, Scott K. Mathematical model for microbial fuel cells with anodic biofilms and anaerobic digestion. Water Sci Technol 2008;57:965–71.
[11] Picioreanu C, Van Loosdrecht MCM, Curtis TP, Scott K. Model based evaluation of the effect of pH and electrode geometry on microbial fuel cell performance. Bioelectrochemistry 2010;78:8–24.
[12] Wen Q, Wu Y, Cao D, Zhao L, Sun Q. Electricity generation and modeling of microbial fuel cell from continuous beer brewery wastewater. Bioresour Technol 2009;100:4171–5.
[13] Zeng Y, Choo YF, Kim BH, Wu P. Modelling and simulation of two-chamber microbial fuel cell. J Power Sources 2010;195:79–89.
[14] Picioreanu C, Head IM, Katuri KP, Van Loosdrecht MCM, Scott K. Modelling microbial fuel cells with suspended cells and added electron transfer mediator. J Appl Electrochem 2010;40:151–62.
[15] Pinto RP, Srinivasan B, Manuel MF, Tartakovsky B. A two-population bio-electrochemical model of a microbial fuel cell. Bioresour Technol 2010;101:5256–65.
[16] Pinto RP, Tartakovsky B, Srinivasan B. Optimizing energy productivity of microbial electrochemical cells. J Process Contr 2012;22:1079–86.
[17] Qi S, Morgenroth E. Modeling steady-state biofilms with dual-substrate limitations. J Environ Eng 2005:320–6.
[18] Oliveira VB, Falcão DS, Rangel CM, Pinto AMFR. Heat and mass transfer effects in a direct methanol fuel cell: a 1D model. Int J Hydrogen Energy 2008;33:3818–28.
[19] Oliveira VB, Rangel CM, Pinto AMFR. One-dimensional and non-isothermal model for a passive DMFC. J Power Sources 2011;196:8973–82.
[20] Sherwood TK, Pigford RL, Wilke CR. Mass transfer. McGraw-Hill; 1975.
[21] Çengel YA. Heat transfer a practical approach. McGraw-Hill; 1998.
[22] O'Hayre R, Cha SK, Colella W, Prinz FB. Fuel cell fundamentals. John Wiley & Sons, Inc; 2006.